Article

Thermal Runaway Vent Gases from High-Capacity Energy Storage LiFePO$_4$ Lithium Iron

Feng Qian [1], Hewu Wang [2,*], Minghai Li [1,*], Cheng Li [2], Hengjie Shen [1], Juan Wang [1], Yalun Li [2] and Minggao Ouyang [2]

[1] School of Mechanical and Engineering, Dalian Jiaotong University, Dalian 116028, China
[2] State Key Laboratory of Automotive Safety and Energy, Tsinghua Universtiy, Beijing 100084, China
[*] Correspondence: wanghw@tsinghua.edu.cn (H.W.); dlminghai8813@djtu.edu.cn (M.L.)

Abstract: Lithium batteries are being utilized more widely, increasing the focus on their thermal safety, which is primarily brought on by their thermal runaway. This paper's focus is the energy storage power station's 50 Ah lithium iron phosphate battery. An in situ eruption study was conducted in an inert environment, while a thermal runaway experiment was conducted utilizing sealed pressure containers and an external heating triggering mechanism. Both the amount of gas release and the battery's maximum temperature were discovered. Using gas chromatography, the gas emission from the battery was examined. Its principal constituents included CO, H$_2$, CO$_2$, CH$_4$, C$_2$H$_4$, and so on. Moreover, the experiment discovered a second eruption of lithium iron phosphate, and the stage of its eruption was separated by the pressure signal of the sealed experimental chamber, giving a theoretical foundation and technological backing for the thermal catastrophe safety of lithium batteries.

Keywords: battery safety; gas analysis; lithium-ion; second eruption; vent gas emission

1. Introduction

In the context of the third energy revolution and carbon neutrality, clean energy technology is rapidly evolving; in particular, energy storage technology, which is typified by the lithium battery, is one of the most rapidly expanding technologies in terms of market capacity in the new energy sector and has been widely adopted [1–5].

As is well recognized, the safe working temperature of lithium batteries should not exceed 80 °C [6]. If the temperature surpasses this, thermal runaway will occur, which is a key issue that affects the safety of the batteries [7]. A lithium battery consists of a positive electrode, a negative electrode, an SEI (solid electrolyte interphase), an electrolyte, etc. [8]. Once thermal runaway of a lithium battery occurs, the surface temperature of the battery will increase quickly, followed by the release of a huge quantity of flammable gas into the atmosphere, which often results in fire, explosion, etc. [9], as well as the accompanying thermal physical phenomena. Studying the flammable gas from a lithium battery eruption [10] may expose the primary cause of lithium electricity fires and offer a foundation for their prevention and control [11].

In recent years, there has been considerable interest in research on high-temperature combustible gas generated by lithium batteries during thermal runaway. Battery gas consists mostly of anode material, electrolyte composition, and a kind of abuse [12,13]. Based on a review of the literature, it can be established that CO$_2$, CO, CH$_4$, and C$_2$H$_4$ are the primary exhaust gas components of lithium-ion batteries, independent of heating abuse or charge and discharge abuse in the experiment [14–18]. In 2005, Doughty [19] found H$_2$ in an ARC (accelerating rate calorimetry) experiment, despite the fact that it was hazardous and could not be detected using conventional detection techniques such as FTIR (Fourier transform infrared spectroscopy). Ohsaki et al. [20] also reported their detection findings in 2005, in which the presence of H$_2$ was discovered via GC (gas chromatography)

in an experiment involving overcharging. Somandepalli [21], Golubkov [15], Lammer [22], and Zheng [23] also discovered H_2. The electrolyte of the battery is composed of DMC (Dimethyl Carbonate), EMC (Ethyl Carbonate), EC (Ethyl Carbonate), or PC (Propylene Carbonate). Studies by Kong, Doughty [19], Abraham [16], Roth, Ribiere, Gachot [14], Sun [18], and others indicate the existence of F-ions in battery gas generation. In a few investigations, C_2H_5F, C_3H_7F, etc., as well as HF and other gases, were identified.

The current study includes effective experimental techniques, outcomes of the primary components of battery gas production, effective gas inspection methods, and some conclusions. Several types of flammable gas emission are summarized. Although there have been significant advances in the current research, there are still some issues. First, there have been few studies on the topic of gas production from lithium batteries with high capacities. Golubkov [24] investigated the gas generation characteristics and dangers of the 18650 lithium battery (1.1 Ah). Second, the experimental methods used to investigate the thermal eruption properties of lithium batteries are not uniform. Wang [25] employed a huge experimental fire platform to explore the eruption and igniting properties, using GC to analyze the gases. Thirdly, the present research focuses on the effects of an eruption's gas output, but the features of gas production have been seldom examined. Weifeng [26] classified the gas generation steps of lithium batteries using conventional internal combustion engine methodology. In addition, flammable gas created by lithium runaway electric heating is the primary cause of fire, but few studies have been conducted on the phase characteristics of lithium battery eruptions. Weifeng [27] recommended studying the mitigation of lithium battery flammable gas using idling technology.

This paper focuses primarily on lithium electric security features, the element of study for the energy storage system in the standard requirement as the anode material of lithium iron phosphate batteries (50 Ah), using constant-volume sealed pressure vessels as experimental tools, and employing inert gas protection technology for the explosion of lithium-ion batteries for in situ gas collection and analysis. This study will explore (1) the temperature-related properties of lithium-ion batteries; (2) the properties of lithium battery gas production; (3) the composition of lithium battery gas generation; and (4) the division of the gas production step for lithium batteries.

2. The Experiment

2.1. Battery Introduction

This study focuses on the 50 Ah lithium iron phosphate battery, which is often used in energy storage systems. It has a rated capacity of 50 Ah, a standard voltage of 3.2 V, a maximum charging voltage of 3.65 V, a discharge termination voltage of 2.5 V, and a mass of 1125 g. Table 1 displays the basic battery specifications.

Table 1. Basic battery information table.

Parameter	Value
Nominal capacity	50 Ah
Cathode material	$LiFePO_4$ (LFP)
Anode material	graphite
Standard voltage	3.2 V
Maximum charging voltage	3.65 V
Initial mass	1125 g
Aging state	fresh, unused
SOC	0%, 50%, 100%

The National Energy Administration suggested in the 25 Key Requirements for Preventing Power Production Accidents (2022 Draft) that NCA ($LiNiAlO_2$) lithium batteries and sodium–sulfur batteries should not be used in medium–large electrochemical energy storage power plants in 2022. Therefore, lithium iron $LiFePO_4$ (LFP) is the optimal material for energy storage power plants.

Lithium iron phosphate batteries include olivine $LiFePO_4$ as the positive electrode, graphite as the negative electrode, and a polymeric substance as the separator. Typically, they are rolled into a sealed metal shell. Li-ions in the positive electrode, pushed by electric field force or concentration difference, traverse the diaphragm and embed themselves into the graphite lattice during charging to create lithium embedment. Li-ions are evacuated from the graphite crystal during discharge, traverse the diaphragm, and return to the surface of the lithium iron phosphate crystal at the positive electrode [28].

2.2. Experiment

In this work, $LiFePO_4$ lithium iron in situ eruption experiments were conducted, primarily in three capacities, namely 100%, 50%, and 0% SOC (state of charge). Thermal runaway does not occur at 0% SOC, according to [29], but the eruption is induced by the side reaction of the electrolyte and other components when the temperature increases. The literature [30] reveals that lithium batteries have a crucial SOC_{CRI}, and batteries below this SOC_{CRI} will not experience thermal runaway. In this experiment, two regularly used capacities, 50% and 100%, were chosen for comparison.

2.2.1. Experimental Setup

In the literature, different researchers who used sealed experimental containers have come to various approaches and results, which are shown in Table 2. Compared to the aforementioned experts, this study is based on their previous research. This experiment was constructed using UL9540, a typical experiment apparatus with a volume of 82 L; a lab made of metal with a seal set; a battery put in the lab, utilizing the cabin environment of heating transfer experiments in the battery; and a test chamber with data on temperature and pressure for analyzing the battery eruption facts.

Table 2. Research status of thermal runaway eruption of lithium-ion batteries.

Related Research	Research Object	Research Contents and Conclusions
Golubkov et al. [25], 2014	18650 battery (LFP and LCO)	Thermal characteristics, maximum temperature, gas production, gas production rate, and composition analysis of lithium battery during thermal runaway.
Somandepalli [18], etc., 2014	2.1 Ah battery ($LiCoO_2$)	Analysis of thermal characteristics, gas production characteristics, gas production components, and explosive characteristics of lithium battery.
S. Koch [28], 2018	20–80 Ah lithium batteries	Analysis of the gas composition, the relationship between the output and the capacity, and the relationship between the temperature and the capacity of lithium battery.
Larsson [29], 2018	6.8 Ah battery $LiCoO_2$	The temperature characteristics of lithium battery eruption, the characteristics of dead battery eruption, the characteristics of eruption products, and the toxicity of eruption products.
Y. Fernandes et al. [12], 2018	2.4 Ah 26650 LFP	Analysis of temperature characteristics of lithium battery eruption and composition of eruption products.
Golubkov et al. [30], 2021	41 Ah lithium battery (Li(NixCoyMnz)O2)	The thermal characteristics, gas production characteristics, and gas production components of lithium battery in different stages.

The experimental principle is depicted in Figure 1. The battery is placed within the experimental apparatus and a sealing device is utilized; the entire experiment is conducted under nitrogen protection. Utilizing specialized technology to arrange cables, all sensors in the experiment are gathered, and the device's pressure sensor is configured for pressure monitoring using pressure and temperature signals for synchronous detection of the eruption's cell facts. A heating device (800wX2) is installed within the experimental apparatus to ensure uniform temperature heating and efficient heat transfer. The actual data collected

after the experiment will eventually take precedence, even if the heater can manage the temperature rise but is unable to precisely predict the pace of heating.
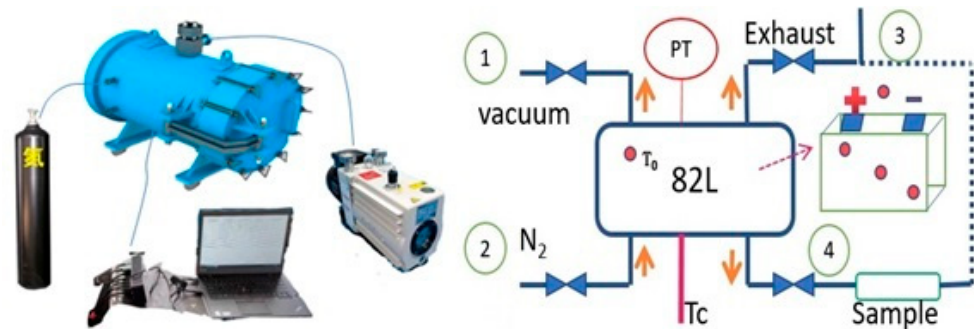

Figure 1. The main component of the experimental apparatus and its principal elements. It consists of the experimental equipment, monitor, vacuum pump, and nitrogen gas cylinder.

2.2.2. Experimental Methods and Steps

First, the experimental preparation of an eruption and experimental procedure is described:

1. The battery capacities for this experiment are 0%, 50%, and 100%.
2. The battery is inserted into the experimental apparatus, and the battery storage bracket is attached to the apparatus (to prevent the battery from dumping). On both sides of the battery, clamps are installed, and the expected force is set to 1–2 N•m.
3. The battery must be positioned vertically so that the safety valve is at the top and it is not dislodged during the eruption.
4. The temperature sensor is put in place, with battery surface temperature Ts, battery safety valve position T50, and battery cabin temperature detection Ta.
5. After securing the experimental apparatus, the experiment is prepared.
6. A vacuum pump is used for vacuum operation (① in Figure 1), and the degree of vacuum is typically −0.8. Nitrogen is then added to the atmospheric pressure ② more than twice.
7. Heating begins and characteristic data are collected using data acquisition. As the ambient temperature rises, so does the temperature of the battery. The pressure of the experimental apparatus is monitored throughout the entire procedure. The increase in pressure indicates that the battery has undergone two processes of eruption and re-eruption. When the battery temperature reaches the thermal runaway temperature and the battery voltage completely fails, the environment heating is turned off until the battery has cooled.
8. The gas collection valve (③ in the experimental principle depicted in Figure 1) is opened.
9. After collecting gas and data, the exhaust valve (④ in the experimental principle depicted in Figure 1) is opened to release exhaust gas, then the sealed container is opened and the battery is removed.

2.2.3. Collection of Temperature Facts

The thermocouple of type K is used for temperature measurement. It is often used due to its stability, affordability, and ease of data collection. The surface temperature of the battery may be measured to determine its temperature at the moment of the initial explosion (safety valve opening). When the battery's temperature rises greatly, the battery undergoes a violent explosion (the second eruption process).

2.2.4. Calculation of Gas Production

The pressure sensor is installed in the sealing test equipment to monitor the pressure in real time, and the gas generation after thermal runaway in the sealed container can be

computed using the pressure and ambient temperature. We computed gas production using the equation for the ideal gas state. The expression is PV = nRT [19].

P (unit Pa) is the internal pressure of the sealing device, V (unit m^3) is its volume, n (unit mol) is the gas output (in mol), R (unit J/(mol·K)) is the ideal gas constant (8.314) [31], and T (unit K) is the ambient temperature of the testing chamber.

2.2.5. Analysis of Gas Composition

A frequently used gas chromatograph, the GC (gas chromatograph), is often used to analyze the composition of gases [25]. In addition, nitrogen was utilized as the background gas in this experiment; therefore, the normalized formula was employed in the calculation of gas components to emphasize the fraction of gas generated by the battery. $Cv = (Cm \times 100)/(100 - C_{N2})$ is the particular normalization formula [27] (C_V represents the volume percentage of a gas, C_M represents the initial proportion of a gas, and C_{N2} represents the nitrogen proportion).

2.2.6. Analyzing Battery Quality Loss

The battery was weighed before and after the experiment using a standard balancing scale. The mass loss of the battery was then computed using the results of the weighing, and the index of mass loss rate was used to determine the intensity of the battery eruption.

3. Experimental Results and Discussion

This experiment employs a brand-new lithium iron $LiFePO_4$ battery used in an energy storage power station. The experiment consists of three SOC capabilities of 100%, 50%, and 0%, and documents the battery temperature, eruption temperature, pressure change, and temperature change in the experimental sealed chamber, battery voltage, and additional data indications for each capacity.

3.1. Recording and Analyzing the Experimental Process

The entire experiment was conducted by heating the heater within the experimental apparatus. The battery transmitted the external temperature to its own heat generation, resulting in thermal runaway. After the battery exploded, the temperature progressively decreased until the conclusion of the experiment. Using the progression of the timeline and the primary data indicators gathered throughout the experiment, a graph depicts the experiment's defining characteristics, as illustrated in the experimental principle depicted in Figure 2. The 100% SOC experimental data are used to show the entire experimental procedure:

0–1500 s: The experimental temperature begins at 25 °C, and the battery voltage is steady at this level. The rate of battery surface temperature rise is around 0.6 °C/min, while the voltage in the testing chamber stays steady.

1500–5000 s: The voltage begins to vary somewhat, but the voltage functioning is still steady at this time. At this point, the increase in cabin temperature is linear. The temperature increases at a rate of around 1.8 °C/min, and the battery surface temperature also rises at a rate of around 1.8 °C/min.

5000–6300 s: The voltage begins to fluctuate significantly, and the vent temperature decreases slightly. Under the pressure of internal electrolyte evaporation, the safety valve opens at this point, allowing a combination of electrolytes and gas to be expelled from the battery at a lower temperature. At this point, the battery's surface temperature remains mostly unchanged, but the experimental chamber's interior pressure undergoes its first abrupt increase, rising to 110 kPa/s.

6300–8000 s: The voltage suddenly drops to 0. An enormous amount of combustible gas explodes at this point; the battery temperature rises quickly, the battery begins thermal runaway, the vent temperature rises quickly, and the pressure inside the experiment chamber abruptly increases once more. This stage is the second stage of battery eruption, and it can be seen from the image that the eruption time is about 500 s.
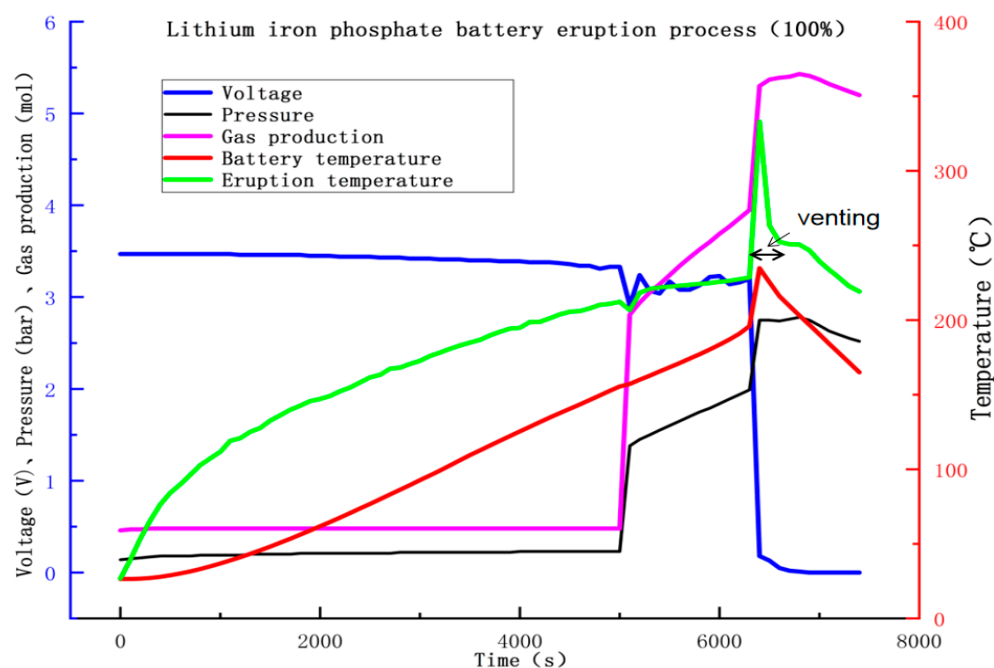
Figure 2. Temperature versus time plot of all temperature and pressure sensors in the pressure vessel. The entire duration of the experiment is shown. A fresh cell at 100% SOC shows the temperatures measured on the cell surface (red) and eruption (green). The cell voltage is plotted in blue. The pressure measured is shown with black line.

Conclusion: According to the data in Figure 3, the nozzle temperature increases with the heating temperature after the beginning of the experiment. Following 1000 s of the experiment, the vent temperature displays a linear rise. The electrolytes are the first thing to be vented when the voltage fluctuates, and when the battery opens the valve, there is a brief drop in vent temperature. When the ambient temperature continues to climb, the voltage suddenly drops to 0, and the battery undergoes thermal runaway. The battery temperature suddenly rises, and the nozzle temperature rises rapidly. There is a violent eruption inside the battery, with an eruption time of about 500 s. The heater of the experimental equipment is stopped, and the temperature in the experimental chamber steadily lowers. After the battery gas is fully mixed with the experimental chamber, gas extraction and analysis operations are conducted.

3.2. Analysis of Temperature Characteristics of Batteries

The thermal hazard of lithium batteries is primarily a result of their chemical energy-driven self-sustaining reaction, which is accompanied by obvious chemical fire characteristics such as high temperature, high heat, smoke, and fire; therefore, temperature-specific analysis is especially vital. The temperature of the battery surface is measured for this experiment, as shown in Figure 4.

According to the experimental data, the battery's temperature increase rate at the beginning of the experiment is 0.6 °C/min, and after 1500 s, its surface temperature rise rate is 2.3 °C/min. When the surface temperature of the battery reaches between 190–210 °C, the thermal regulation of the battery is activated, the temperature increase rate accelerates to 37 °C/min, and the voltage decreases to zero instantly. Eventually, the battery temperature reaches a maximum of around 320 °C. After, while external heating is still present, the battery temperature will progressively decline, albeit at a sluggish rate, since the battery experienced an explosion after the positive and negative chemical reactions.
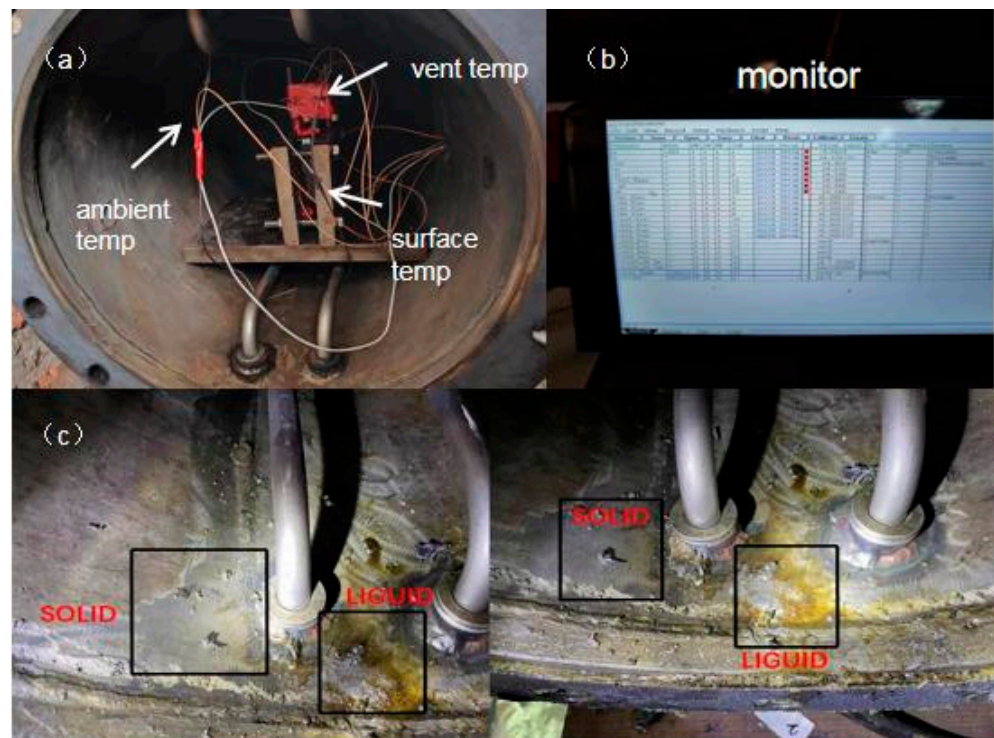
Figure 3. Photos of the experiment show how the temperature sensor was arranged and the residue that was left within the experimental equipment after the experiment. (**a**) Schematic diagram of temperature sensor. (**b**) Schematic diagram of data parameter monitoring. (**c**) Schematic diagram of the interior of the chamber after the experiment.
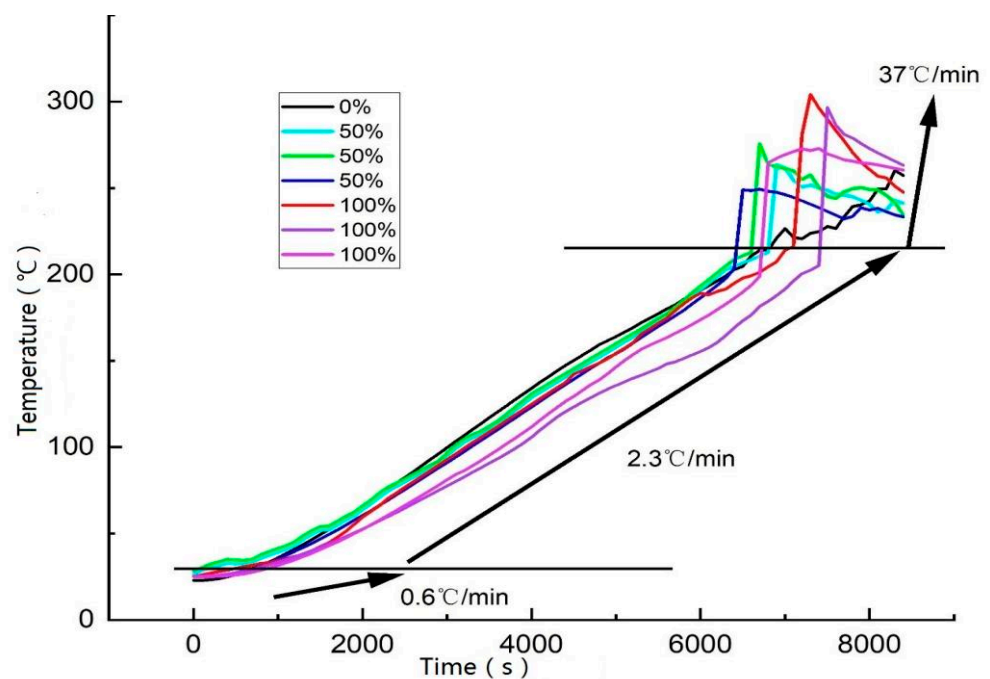

Figure 4. Temperature rate of the cell versus cell temperature. Overview of the entire experiment duration. A fresh cell at 100%, 50%, and 0% SOC shows the temperatures measured on the cell surface. The rate of temperature rise is divided into three stages, 0.6 °C/min, 2.3 °C/min, 37 °C/min.

The rates of temperature increase and rise are plotted (Figure 4). Although the temperature increase rate is rapid, the temperature rise rate of the battery does not vary much,

demonstrating that lithium iron phosphate batteries are reasonably safe. A tangent with multiple stages of temperature rise rate can be found in the vicinity of 160 °C at the junctures, as shown in Figure 5; the valve of the battery temperature and the temperature point opens, and the battery is in the open after going through the process of temperature rise in the valve, reaching the eruption process. It can be seen from this angle that the lithium iron phosphate battery valve opens before thermal runaway.
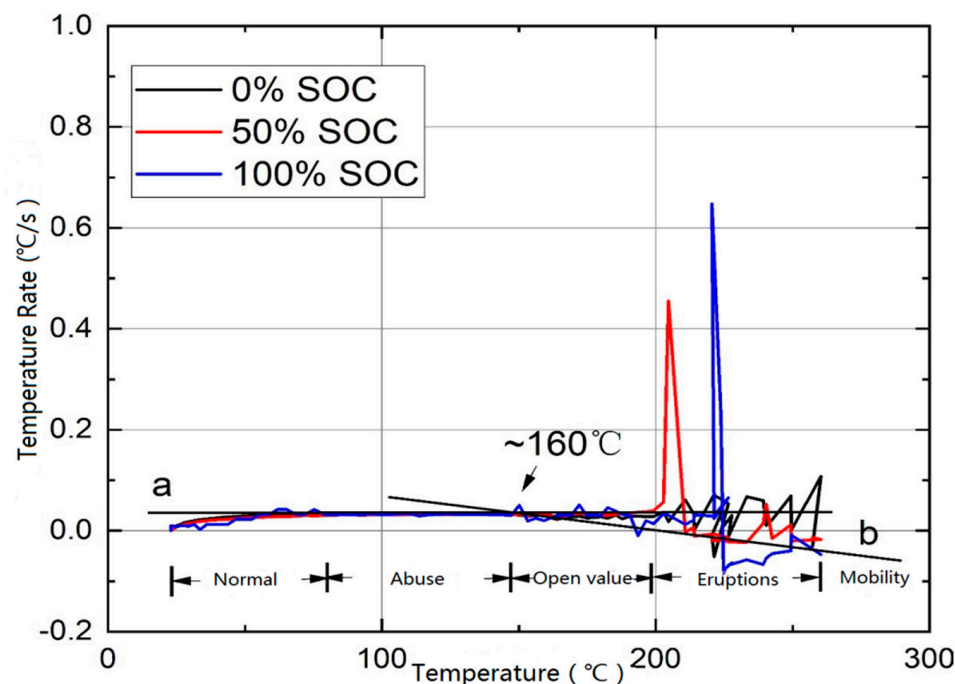

Figure 5. Temperature rate of the cell versus cell temperature. The stages of thermal runaway are divided. The thermal runaway behavior of the battery is divided into several phases depending on the variation in temperature rise rate. The thermal runaway reaction begins at the point where the two lines intersect, which is roughly 160 °C.

3.3. Analysis of Gas Production Characteristics

The increase in the temperature of the battery's surface will result in heat propagation and the occurrence of a thermal disaster [32], while the explosion caused by overpressure inside the battery [33] is also one of the reasons that contribute to the more severe propagation of thermal disaster. Using the inert gas protection technology given in this experiment, the properties of the battery safety valve after an explosion may be seen more clearly. As the battery's safety valve, a weak shrapnel is often positioned immediately above the battery and between the positive and negative poles for aluminum-shell batteries. Typically, shrapnel can resist pressures between 0.5 and 0.8 bar [34]. When the pressure produced by the reaction within the battery exceeds the pressure carried by the shrapnel, the safety valve will open and release flammable gas and a portion of the electrolyte, as well as the positive and negative compounds created inside the battery. There is no combustion in the battery test chamber due to the nitrogen protection. The flammable gas combines with nitrogen in the experimental chamber and grows as the experiment progresses, causing the chamber's pressure to rise proportionally.

The ideal gas equation of state is used to compute the mol of the gas mixture, which represents the molar mass of the erupting mixture. To analyze the characteristics of gas generation, refer to Figure 6, which represents the change in mol quantity during battery eruption. Even if the starting amount of gas in the experimental equipment does not change much and the nitrogen expands little as the temperature climbs, the expansion result may be ignored. After a rapid decrease in voltage, the molar mass in the experimental chamber rises quickly, and after a rapid decrease in voltage to zero, the molar mass rises abruptly and reaches

its maximum. Before and after the experiment, the change in molar mass in the chamber was used to calculate the amount of combustible gas mixture that the battery discharged.
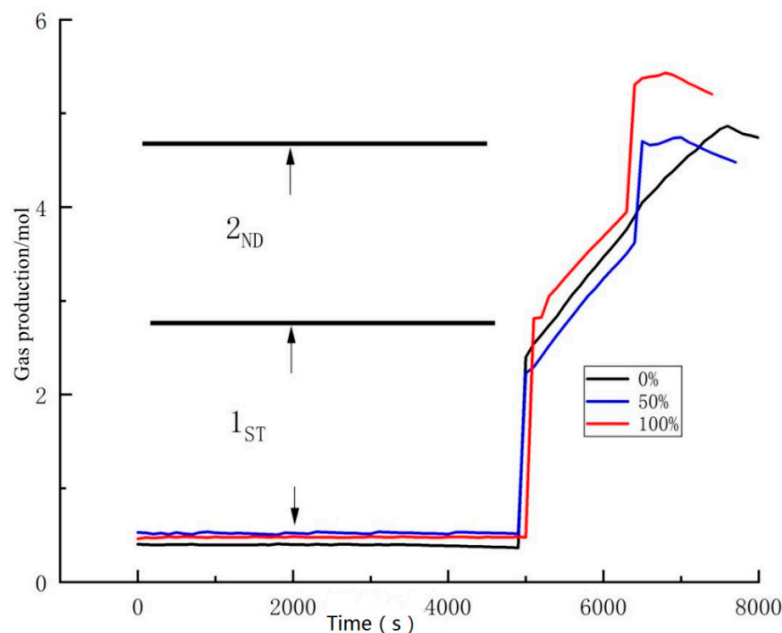

Figure 6. Amount of produced gas versus time plot under 0%, 50%, and 100% SOC. When the quantity of gas produced by the battery is calculated using the equation of state for ideal gases law it is obvious that the eruption occurs in two phases.

3.4. Composition Analysis of Gas Production

The emission of lithium batteries caused by thermal runaway is also one of the causes of a thermal catastrophe. Thermal runaway in lithium batteries is followed by the release of electrolytes and both positive and negative reactions. Electrolytes (EC, EMC, etc.) and other gases (CO_2, CH_4, H_2, O_2, CO) generated by other processes are included in the emission. In this experiment, the experimental apparatus was utilized to collect and examine the products. Figure 7 depicts the product composition and analytical findings.
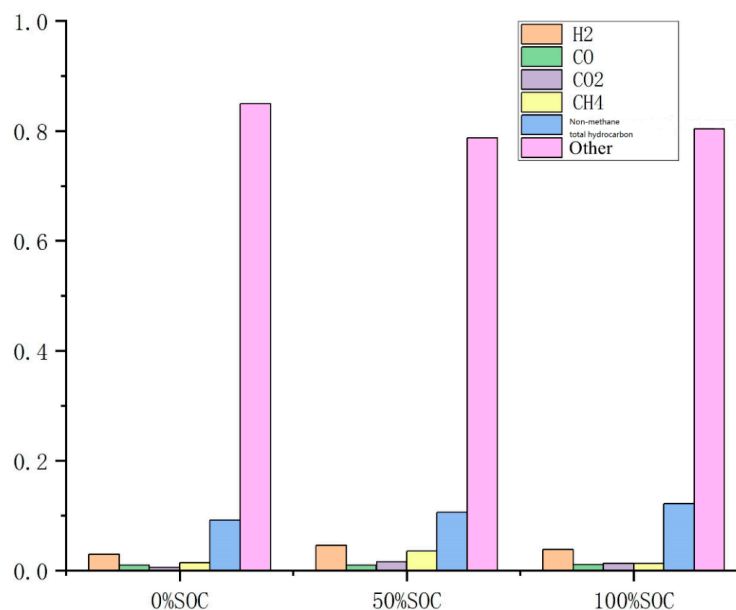

Figure 7. Detected components of the produced gases (%). The principal constituents included CO, H_2, CO_2, CH_4, and C_2H_4. Other ingredients included small amounts of water, EMC, and so on [16–19].

As indicated in Figure 7, the experimental findings were normalized and produced via analysis since all of the trials were conducted against a nitrogen background and there were around 25 low-composition nonmethane hydrocarbons. The primary components are CO_2, CH_4, H_2, and CO, with H_2 being one of the most flammable gases, thus affecting the safety of lithium iron batteries, as shown in Figure 8.
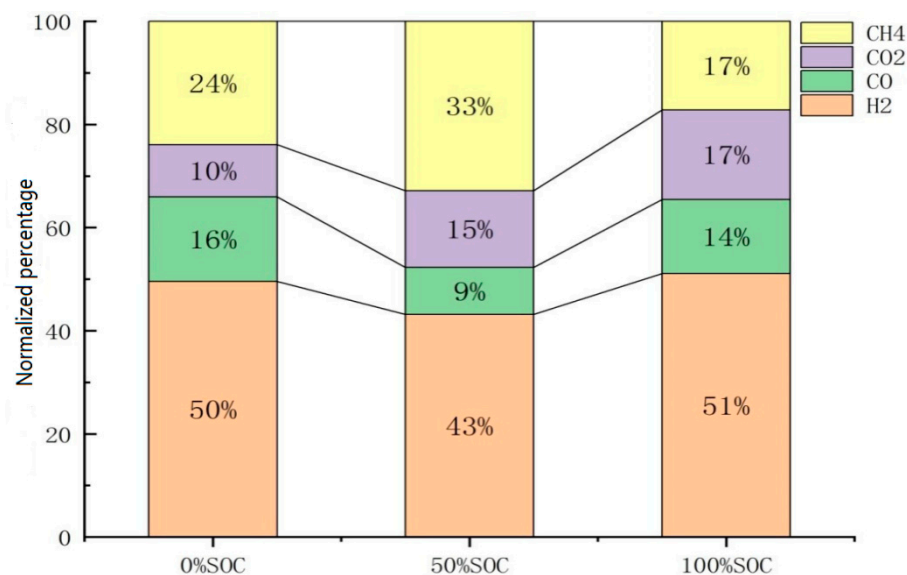

Figure 8. Normalized percentage of lithium iron gas production constituents. From the perspective of gas production, H_2 accounts for a relatively high proportion of the gas generated by lithium iron phosphate batteries, approaching about 50%.

Before each experiment, the weight of the battery was measured. This experiment was conducted with 0% SOC, 50% SOC, and 100% SOC capacity. The initial mass of the sample battery was 1125 g. The weight of the battery was measured using the formula $R = (M_O − M_{END})/M_O$ (R is the mass loss rate, M_O is the original weight, and M_{END} is the residual weight), and the mass loss rate may be calculated using Table 3. This loss is mostly evident in the creation of gas, the loss of electrolytes, and the loss of positive and negative electrode materials.

Table 3. Mass loss rate of lithium iron phosphate battery in eruption experiment.

	0%	50%	100%
Original weight (g)	1125	1125	1125
Residual weight (g)	949	936	918
Rate of mass loss	16%	17%	18%

3.5. Division of Lithium Battery Gas Production

According to experimental research, lithium electric heat damage results primarily from its own production releases of heat and thermal runaway of combustible gas, and because the lithium battery inside the open valve reacts to the pressure and the external battery has no apparent gases, the battery's internal pressure opens the valve, the relief valve opens, and electrolytes and gas are released.

When thermal runaway develops, the battery will aggressively emit flammable smoke before reaching a stable state of failure. As seen in Figure 9, the gas generation stage of the battery may be clearly differentiated by the pressure index of the sealed experimental apparatus.
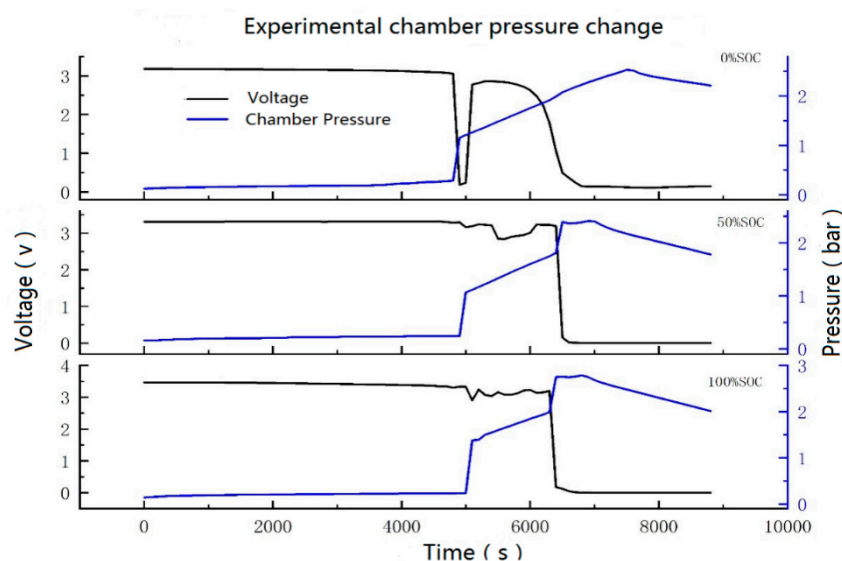
Figure 9. Pressure change curve of experimental chamber, showing two stages of eruption. At 0% SOC, the battery valve was opened and there was no major secondary eruption. A second eruption occurred at 50% and 100% SOC, and the manifested traits are largely constant.

No gas release stage: stable voltage, stable pressure.
First valve opening: voltage fluctuation, pressure surge.
Second eruption: voltage surge, pressure surge again.
Gas flow: voltage disappears, pressure drops slowly.
The three-phase gas–liquid–solid substances produced by the battery are responsible for the pressure increase in the testing chamber. The ideal gas equation may be used to determine the mol quantity of substances:

$$n_{sum} = \frac{pV}{RT} - n_0$$

where n_{sum} is the total mass produced, p is the experimental device's pressure, V is its volume, R is the gas constant, T is the surrounding temperature, and n_0 is the mass of the starting material. As demonstrated in Figure 10, the link between the battery product state and the battery temperature stage may be observed by comparing the gas state with the battery surface temperature.

Closed valve area: The battery's temperature ranges from 25 to 160 °C. At this point, the battery has had a response, but the gas volume is low and the safety valve's opening pressure has not been exceeded. The gas production efficiency is steady, and there is no noticeable temperature increase.

First eruption area: The battery's temperature ranges from 160 to 200 °C. At this point, a small amount of gas leaks out because the pressure needed to open the safety valve is greater than the gas production pressure inside the battery. The temperature of the nozzle (Figure 4) exhibits a sharp decline at this point because the temperature of the material being ejected is lower than the surrounding air temperature.

Second eruption zone: The temperature of the battery ranges from 200 to 300 °C. At this point, a considerable quantity of gas is expelled from the battery as a result of a strong reaction. At this point, the battery temperature reaches its maximum, and the quantity of gas also reaches its maximum and becomes steady.

Gas-producing flow area: At this point, the battery temperature decreases and the reaction within the battery is complete. The temperature does not increase, and power decreases. There is no gas overflow inside the battery, and it fails entirely.
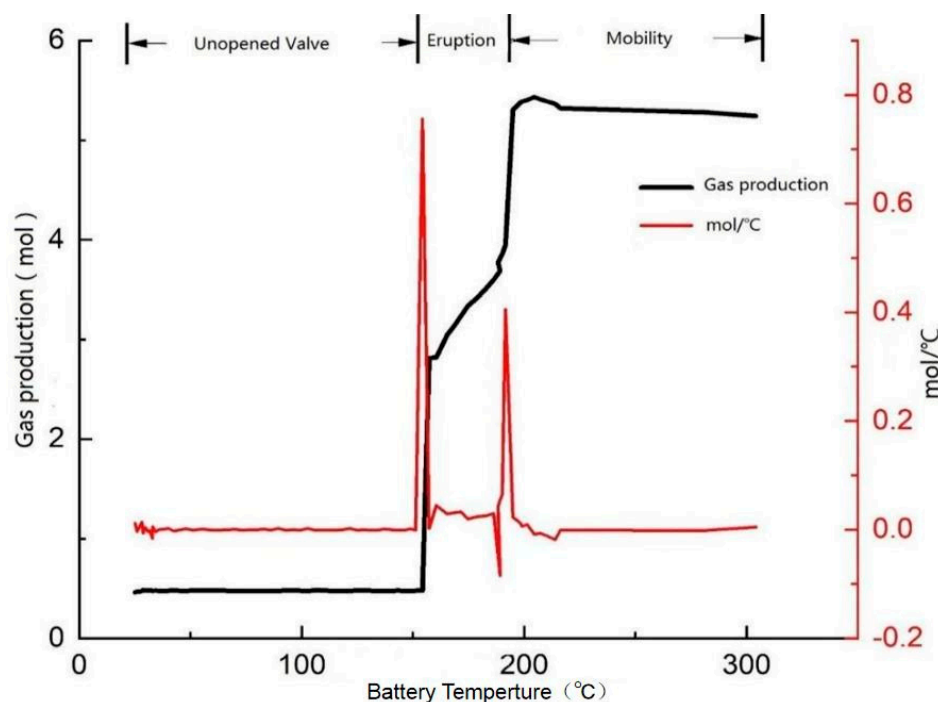
Figure 10. Gas production of the cell versus cell temperature. Stages of battery gas generation are divided. Following the initial valve opening, the temperature-dependent gas production steadily rises.

3.6. Discussion

We summarize the above experimental findings as follows, after conducting an extensive study and comparison of the characteristics received from the entire experiment:

1. The severity of the thermal runaway increased with increasing SOC, as shown by the graphic in Figure 4, 100% TMAX > 50% TMAX > 0% TMAX.

2. According to research in relevant literature [15], charged NCA cells showed a drastic thermal runaway behavior. NCA cells can reach maximum temperatures of 1075 °C. In this study, LFP cells exhibited a less pronounced thermal runaway with maximum cell temperatures as high as 305 °C.

3. LFP clearly exhibits two-stage eruption phenomena, which is essentially compatible with the description in other pertinent articles [22]. From the perspective of gas production, H2 accounts for a relatively high proportion of the gas generated by lithium iron phosphate batteries, approaching about 50%.

4. Summary and Outlook

4.1. Conclusions

A thermal runaway experiment was conducted using a 50 Ah lithium iron phosphate battery with an aluminum lid. The whole eruption procedure was carried out in enclosed laboratory equipment. Following the experiment, the thermal characteristics of the collected gas were examined. Using GC gas analysis, the components of the gas were measured. This may be summarized as follows:

(1) The secondary eruption of a lithium iron phosphate battery will occur around 20 min after the opening of the valve. The initial valve opening is accompanied by a modest quantity of electrolyte and gas.

(2) During thermal runaway, the surface temperature of the batteries is around 190 °C, and the peak temperature does not exceed 350 °C, which is substantially lower than that of ternary batteries.

(3) The battery will emit around 4.5 mol of gaseous pollutants. CO_2, CH_4, H_2, and CO are the gases with the highest volume %, as determined by the GC-MS apparatus, with CH_4, H_2, and CO being combustible and CO containing a specific level of toxicity.

(4) The mass loss rate of the batteries is between 18 to 20%, with the majority of lost products being electrolytes. Comparatively, ternary products are mostly solid powders.

(5) Lithium batteries provide a thermal risk that spreads via transmission and dissemination, particularly with the propagation of flammable flue gas. The thermal danger of the battery is separated according to the stage of gas generation, and the parameters of each step are provided.

4.2. Outlook

Through ongoing tests and analyses, the thermal degradation of lithium batteries must be studied. The use of lithium batteries has changed from electric cars to energy storage goods, and batteries with a medium load state will be replaced by batteries with a higher capacity. Consequently, it is crucial to develop a set of research methodologies for lithium batteries.

(1) In research on high-capacity lithium batteries, particular attention must be paid to the experiment's safety, particularly with regards to the battery at the module level.

(2) Based on the examination of the study findings, H_2 and other common gases are one of the future research foci, with flammable and hazardous gases being of particular importance.

(3) Because the thermal runaway temperature of a lithium iron phosphate battery is not high and the process of two eruptions is protracted, the next research path is to determine if there is a mechanism to halt abuse or avoid the onset of thermal runaway and its boundaries.

(4) One of the primary reasons of lithium fire, which has intricate fire components, continuous self-generated battery heat, and significant flue gas mobility, is the flammable smoke that results from the eruption of lithium batteries. The attention then shifts to fire warning and fire rescue procedures.

Author Contributions: Conceptualization, F.Q.; funding acquisition, M.O.; methodology, F.Q., C.L., H.S. and J.W.; project administration, H.W., Y.L. and M.O.; software, F.Q., J.W. and Y.L.; supervision, H.W., H.S., Y.L. and M.O.; validation, H.W., M.L. and J.W.; visualization, F.Q., C.L. and Y.L.; writing—original draft, F.Q., H.W. and Y.L.; writing—review and editing, F.Q., H.W., M.L. and Y.L. All authors have read and agreed to the published version of the manuscript.

Data Availability Statement: The data are available through appropriate requests.

Conflicts of Interest: The authors declare no conflict of interest.

References

1. Zaghib, K.; Dubé, J.; Dallaire, A.; Galoustov, K.; Guerfi, A.; Ramanathan, M.; Benmayza, A.; Prakash, J.; Mauger, A.; Julien, C.M. Enhanced thermal safety and high power performance of carbon-coated LiFePO$_4$ olivine cathode for Li-ion batteries. *J. Power Sources* **2012**, *219*, 36–44. [CrossRef]
2. Song, Z.; Yang, X.; Yang, N.; Delgado, F.P.; Hofmann, H.; Sun, J. A Study of Cell-to-Cell Variation of Capacity in Parallel-Connected Lithium-Ion Battery Cells. *eTransportation* **2021**, *7*, 100091. [CrossRef]
3. Feng, X.; Sun, J.; Ouyang, M.; Wang, F.; He, X.; Lu, L.; Peng, H. Characterization of penetration induced thermal runaway propagation process within a large format lithium ion battery module. *J. Power Sources* **2015**, *275*, 261–273. [CrossRef]
4. Li, Y.; Wei, Y.; Zhu, F.; Du, J.; Zhao, Z.; Ouyang, M. The path enabling storage of renewable energy toward carbon neutralization in China. *eTransportation* **2023**, *16*, 100226. [CrossRef]

5. Wang, X.; Wei, X.; Zhu, J.; Dai, H.; Zheng, Y.; Xu, X.; Chen, Q. A review of modeling, acquisition, and application of lithium-ion battery impedance for onboard battery management. *eTransportation* **2021**, *7*, 100093. [CrossRef]

6. Feng, X.; Ren, D.; He, X.; Ouyang, M. Mitigating Thermal Runaway of Lithium-Ion Batteries. *Joule* **2020**, *4*, 743–770. [CrossRef]

7. Feng, X.; Ouyang, M.; Liu, X.; Lu, L.; Xia, Y.; He, X. Thermal runaway mechanism of lithium ion battery for electric vehicles: A review. *Energy Storage Mater.* **2018**, *10*, 246–267. [CrossRef]

8. Kvasha, A.; Gutiérrez, C.; Osa, U.; Iratxe de Meatza, J.; Blazquez, A.; Macicior, H.; Urdampilleta, I. A comparative study of thermal runaway of commercial lithium ion cells. *Energy* **2018**, *159*, 547–557. [CrossRef]

9. Liu, K.; Liu, Y.; Lin, D.; Pei, A.; Cui, Y. Materials for lithium-ion battery safety. *Sci. Adv.* **2018**, *4*, 9820. [CrossRef] [PubMed]

10. Wen, C.-Y.; Jhu, C.-Y.; Wang, Y.-W.; Chiang, C.-C.; Shu, C.-M. Thermal runaway features of 18650 lithium-ion batteries for LiFePO$_4$ cathode material by DSC and VSP2. *J. Therm. Anal. Calorim.* **2012**, *3*, 1297–1302. [CrossRef]

11. Qin, P.; Sun, J.; Yang, X.; Wang, Q. Battery thermal management system based on the forced-air convection: A review. *eTransportation* **2020**, *7*, 100097. [CrossRef]

12. Fernandes, Y.; Bry, A.; de Persis, S. Identification and quantification of gases emitted during abuse tests by overcharge of a commercial Li-ion battery. *J. Power Sources* **2018**, *389*, 106–119. [CrossRef]

13. Wen, J.; Yu, Y.; Chen, C. A Review on Lithium-Ion Batteries Safety Issues: Existing Problems and Possible Solutions. *Mater. Express* **2012**, *3*, 197–212. [CrossRef]

14. Gachot, G.; Ribiere, P.; Mathiron, D.; Grugeon, S.; Armand, M.; Leriche, J.-B.; Pilard, S.; Laruelle, S. Gas Chromatography/Mass Spectrometry As a Suitable Tool for the Li-Ion Battery Electrolyte Degradation Mechanisms Study. *Anal. Chem.* **2011**, *2*, 478–485. [CrossRef]

15. Golubkov, A.W.; Scheikl, S.; Planteu, R.; Voitic, G.; Wiltsche, H.; Stangl, C.; Hacker, V. Thermal runaway of commercial 18650 Li-ion batteries with LFP and NCA cathodes—impact of state of charge and overcharge. *RSC Adv.* **2015**, *70*, 57171–57186. [CrossRef]

16. Abraham, D.P.; Roth, E.P.; Kostecki, R.; McCarthy, K.; MacLaren, S.; Doughty, D.H. Diagnostic examination of thermally abused high-power lithium-ion cells. *J. Power Sources* **2006**, *1*, 648–657. [CrossRef]

17. Fu, Y.; Lu, S.; Li, K.; Liu, C.; Cheng, X.; Zhang, H. An experimental study on burning behaviors of 18650 lithium ion batteries using a cone calorimeter. *J. Power Sources* **2015**, *273*, 216–222. [CrossRef]

18. Sun, J.; Li, J.; Zhou, T.; Yang, K.; Wei, S.; Tang, N.; Dang, N.; Li, H.; Qiu, X.; Chen, L. Toxicity, a serious concern of thermal runaway from commercial Li-ion battery. *Nano Energy* **2016**, *27*, 313–319. [CrossRef]

19. Doughty, D.H.; Roth, E.P.; Crafts, C.C.; Nagasubramanian, G.; Henriksen, G.; Amine, K. Effects of additives on thermal stability of Li ion cells. *J. Power Sources* **2005**, *146*, 116–120. [CrossRef]

20. Ohsaki, T.; Kishi, T.; Kuboki, T.; Takami, N.; Shimura, N.; Sato, Y.; Sekino, M.; Satoh, A. Overcharge reaction of lithium-ion batteries. *J. Power Sources* **2005**, *146*, 97–100. [CrossRef]

21. Somandepalli, V.-S.-R.; Marr, K.-C.; Horn, Q.-C. Quantification of Combustion Hazards of Thermal Runaway Failures in Lithium-Ion Batteries. *SAE Int. J. Alt. Power.* **2014**, *3*, 98–104. [CrossRef]

22. Lammer, M.; Konigseder, A.; Hacker, V. Holistic methodology for characterisation of the thermally induced failure of commercially available 18650 lithium ion cells. *RSC Adv.* **2017**, *39*, 24425–24429. [CrossRef]

23. Zheng, Y.; Qian, K.; Luo, D.; Li, Y.; Lu, Q.; Li, B.; He, Y.-B.; Wang, X.; Li, J.; Kang, F. Influence of over-discharge on the lifetime and performance of LiFePO$_4$/graphite batteries. *RSC Adv.* **2016**, *36*, 30474–30483. [CrossRef]

24. Andrey, W.G.; Fuchsa, D.; Wagnerb, J.; Wiltschec, H.; Stangld, C.; Faulerd, G.; Voitice, G.; Thalera, A.; Hackere, V. Thermal-runaway experiments on consumer Li-ion batteries with metal-oxide and olivin-type cathodes. *RSC Adv.* **2014**, *7*, 3633–3642.

25. Wang, Q.; Ping, P.; Zhao, X.; Chu, G.; Sun, J.; Chen, C. Thermal runaway caused fire and explosion of lithium ion battery. *J. Power Sources* **2012**, *208*, 210–224. [CrossRef]

26. Li, W.; Wang, H.; Ouyang, M.; Xu, C.; Lu, L.; Feng, X. Theoretical and experimental analysis of the lithium-ion battery thermal runaway process based on the internal combustion engine combustion theory. *Energ. Convers. Manag.* **2019**, *185*, 211–222. [CrossRef]

27. Li, W.; Wang, H.; Zhang, Y.; Ouyang, M. Flammability characteristics of the battery vent gas: A case of NCA and LFP lithium-ion batteries during external heating abuse. *J. Energy Storage* **2019**, *24*, 100775. [CrossRef]

28. Zhang, Y.; Wang, H.; Li, W.; Li, C.; Ouyang, M. Quantitative analysis of eruption process of abused prismatic Ni-rich automotive batteries based on in-chamber pressure. *J. Energy Storage* **2020**, *31*, 101617. [CrossRef]

29. Huang, P.; Yao, C.; Mao, B.; Wang, Q.; Sun, J.; Bai, Z. The critical characteristics and transition process of lithium-ion battery thermal runaway. *Energy* **2020**, *213*, 119082. [CrossRef]

30. Essl, C.; Golubkov, A.W.; Gasser, E.; Nachtnebel, M.; Zankel, A.; Ewert, E.; Fuchs, A. Comprehensive Hazard Analysis of Failing Automotive Lithium-Ion Batteries in Overtemperature Experiments. *Batter. Basel* **2020**, *6*, 30. [CrossRef]

31. Zhang, Y.; Wang, H.; Wang, Y.; Li, C.; Liu, Y.; Ouyang, M. Thermal abusive experimental research on the large-format lithium-ion battery using a buried dual-sensor. *J. Energy Storage* **2021**, *33*, 102156. [CrossRef]

32. Li, C.; Wang, H.; Han, X.; Wang, Y.; Wang, Y.; Zhang, Y.; Feng, X.; Ouyang, M. An Experimental Study on Thermal Runaway Behavior for High-Capacity Li(Ni$_{0.8}$Co$_{0.1}$Mn$_{0.1}$)O$_2$ Pouch Cells at Different State of Charges. *J. Electrochem. En. Conv. Stor.* **2021**, *2*, 021012. [CrossRef]

33. Wang, Y.; Wang, H.; Zhang, Y.; Li, C.; Wu, Y.; Feng, X.; Lu, L.; Ouyang, M. Thermal oxidation characteristics for smoke particles from an abused prismatic $Li(Ni_{0.6}Co_{0.2}Mn_{0.2})O_2$ battery. *J. Energy Storage* **2021**, *39*, 102639. [CrossRef]
34. Zhang, Y.; Wang, H.; Li, W.; Li, C.; Ouyang, M. Size distribution and elemental composition of vent particles from abused prismatic Ni-rich automotive lithium-ion batteries. *J. Energy Storage* **2019**, *26*, 100991. [CrossRef]